Artificial bacterial flagella: Fabrication and magnetic control

Li Zhang,[1] Jake J. Abbott,[1,2] Lixin Dong,[1,3] Bradley E. Kratochvil,[1] Dominik Bell,[1] and Bradley J. Nelson[1,a)]
[1]*Institute of Robotics and Intelligent Systems, ETH Zurich, CH-8092 Zurich, Switzerland*
[2]*Department of Mechanical Engineering, University of Utah, Salt Lake City, Utah 84112, USA*
[3]*Department of Electrical and Computer Engineering, Michigan State University, East Lansing, Michigan 48824, USA*

(Received 21 October 2008; accepted 19 January 2009; published online 13 February 2009)

Inspired by the natural design of bacterial flagella, we report artificial bacterial flagella (ABF) that have a comparable shape and size to their organic counterparts and can swim in a controllable fashion using weak applied magnetic fields. The helical swimmer consists of a helical tail resembling the dimensions of a natural flagellum and a thin soft-magnetic "head" on one end. The swimming locomotion of ABF is precisely controlled by three orthogonal electromagnetic coil pairs. Microsphere manipulation is performed, and the thrust force generated by an ABF is analyzed. ABF swimmers represent the first demonstration of microscopic artificial swimmers that use helical propulsion. Self-propelled devices such as these are of interest in fundamental research and for biomedical applications. © *2009 American Institute of Physics*. [DOI: 10.1063/1.3079655]

The controlled locomotion of untethered microrobots in a liquid environment is of interest both fundamentally and for biomedical applications. Previous work has shown that the use of external magnetic fields for propelling millimeter and micrometer scale robotic agents in liquid via wireless energy transfer is effective.[1–5] However, all of these agents are still several orders-of-magnitude larger than natural microscopic organisms such as bacteria. Bacteria, like many microorganisms, swim in liquid using flagella. Flagellar mechanisms are particularly well suited to the low-Reynolds-number environment in which they live because of their ability to generate nonreciprocating motion.[6] Inspired by monotrichous bacteria flagella, we report the fabrication and controlled swimming of artificial bacterial flagella (ABF). These helical devices precisely locomote using controlled, low-strength, rotating magnetic fields using the same low-Reynolds-number swimming strategy[6] that evolved in bacteria billions of years ago.

An ABF consists of the two following parts: a helical tail resembling a natural flagellum in both size and shape and a soft-magnetic metal head in the shape of a thin square plate. We use the terms "tail" and "head" loosely, as the ABF swimmers have no preferred forward orientation. The fabrication of the ABF is mainly based on a self-scrolling technique.[7–10] First, an AlGaAs sacrificial layer and an InGaAs/GaAs bilayer are epigrown on a GaAs (001) wafer by molecular beam epitaxy. After the deposition of a 15 nm Cr layer by e-beam evaporation, the InGaAs/GaAs/Cr trilayer is patterned to a ribbonlike mesa for the helical tail by reactive ion etching. Then, the soft-magnetic head is prepared by e-beam evaporation of Cr/Ni/Au thin films and a lift-off process. Finally, the AlGaAs sacrificial layer is selectively etched by 2% HF aqueous solution to release the patterned mesa, on which the two-dimensional patterned films self-organize to form an ABF. After the "top-down" fabrication processes, the entire patterned mesa is released from the substrate and automatically scrolls into an ABF, as shown in Figs. 1(a)–1(f). In the experiments, two different types of ABF have been prepared. One has an InGaAs/GaAs semiconductor bilayer tail and the other has the InGaAs/GaAs/Cr hybrid semiconductor-metal trilayer tail described above. It was found that the InGaAs/GaAs/Cr helical tail has the advantage that it is more robust than the bilayer helical tail for the manipulation step required to place the ABF in liquid. For the experiments, the InGaAs/GaAs bilayer and InGaAs/GaAs/Cr trilayer have thicknesses of 11/16 nm and 11/16/15 nm, respectively, the ribbon width is 1.8 μm, and the diameter of the as-fabricated InGaAs/GaAs and InGaAs/GaAs/Cr ABF are 2.6 and 2.8 μm, respectively. Different materials are candidates for helical tail fabrication, including semiconductors, metals, and polymers.[7,8,11] The soft-magnetic metal head is in the shape of a thin square plate with dimensions of 4.5 μm (length) $\times$ 4.5 μm (width) $\times$ 200 nm (thickness). It is composed of a Cr/Ni/Au trilayer with a thickness of 10/180/10 nm, respectively. The geometrical shape of the helical tail (e.g., chirality, helicity angle, and diameter) can be precisely controlled as reported previously.[10] Figure 1(g) shows a field emission scanning electron microscopy (FESEM) micrograph of an untethered ABF with InGaAs/GaAs/Cr helical tail. To untether the ABF from the substrate, micromanipulation is performed to cut, pick, and release the ABF. Micromanipulation of the ABF was performed in the following way. First, an ABF is cut from the substrate using a tungsten probe mounted on a manipulator (Signatone model S-926) under an optical microscope. The radius of the probe tip is approximately 100 nm. Due to van der Waals forces, the ABF sticks to the probe. Then the ABF is transferred from the GaAs surface by moving the manipulator probe above a smooth SiO_2 surface. The ABF is released into solution by tapping the manipulator. Finally, a rotating magnetic field is applied to drive the ABF. The reservoir for swimming experiments has a dimension of 20 mm (length) $\times$ 15 mm (width) $\times$ 2 mm (height), and the sample is immersed in deionized water with a viscosity of 1 mPa/s. For precise control of the motion of the ABF, three pairs of orthogonal electromagnetic coils were constructed to generate a uniform rotating magnetic field, as shown in Fig. 2. Our setup requires no special modification of the probe station (Signatone model S-1160). The coils are simply placed around the

a)Electronic mail: bnelson@ethz.ch.

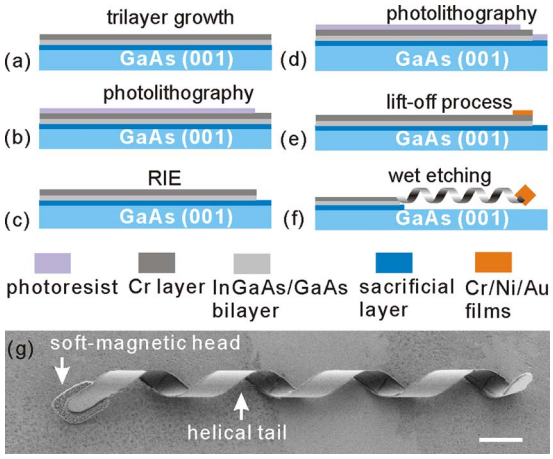

FIG. 1. (Color online) [(a)–(f)] Fabrication procedure of the ABF with InGaAs/GaAs/Cr helical tail. (g) FESEM image of an untethered ABF. The scale bar is 4 μm.

lens. The four following parameters can be independently controlled in the software by the user: the magnetic field strength, the rotational frequency of the field, and the yaw and pitch of the ABF swimmer. Field strength of 2.0 mT is generated in the working region of the electromagnetic coils. After the micromanipulation step, the electromagnetic fields are activated to drive the ABF.

For forward and backward motion the ABF acts as a helical propeller to convert rotary motion to linear motion, as shown in Figs. 3(a) and 3(b), thus forward and backward motion can be switched by simply reversing the rotation direction, i.e., by rotating the magnetic field clockwise (with an observer in front of the ABF), a left-handed ABF swims forward, and by rotating the field counterclockwise, it moves backward. The magnetic torque for rotation is generated by the thin head attempting to align with the applied field, as shown in Figs. 3(c) and 3(d). In Fig. 3(e), a series of frames of an ABF, which has a left-handed chirality and a tail length of 47 μm, swims forward by rotating the magnet field clockwise (as seen by an observer in front of the ABF) until $t=8$ s, and then the ABF reverses direction by rotating the field counterclockwise. In contrast to reversing motion by turning the swimmer 180°, which is the method used by bacteria and existing microscopic artificial swimmers,[12] reversing the rotation direction is a more straightforward and time-efficient method.

In addition to a magnetic torque for propulsion, there is a magnetic torque generated for steering. It has been reported that in a weak applied field the easy magnetization axes of a thin square plate are along the diagonals.[13] It is also known that magnetic torque will tend to align an easy axis with the applied field. Although there are two possible easy axes in a square plate [i.e., $\overline{ac}$ and $\overline{bd}$ in Figs. 3(f) and 3(g)], the one that is closer to the applied field will act as the easy axis [i.e., $\overline{ac}$ in Fig. 3(f) and $\overline{bd}$ in Fig. 3(g)]. We ensure that the diagonal $\overline{ac}$, which is perpendicular to the axis of the ABF helix, becomes the magnetized axis during normal swimming. When the magnetic field is misaligned by less than 45° with respect to this easy axis [i.e., $|\gamma|<45°$ in Fig. 3(f)], the magnetic head attempts to align $\overline{ac}$ to the external field as the helix rotates axially. When the other diagonal is closer to the magnetic field [i.e., $|\gamma|<45°$ in Fig. 3(g)], the diagonal $\overline{bd}$ becomes magnetized and the ABF attempts to rotate perpendicular to the helix axis, which is undesirable during swimming, but is useful for orienting a stationary ABF. Figure 3(h) shows a series of an ABF turning 70° in 5 s.

For the user interface, two steering parameters are controlled: pitch, which is the angle of the ABF helix axis with respect to the horizontal plane; and yaw, which is the angle of the ABF helix axis observed in the horizontal imaging plane. Although inertial effects of ABF are negligible and ABF reach their steady-state velocities in water nearly instantaneously, the weight of an ABF must be taken into ac-

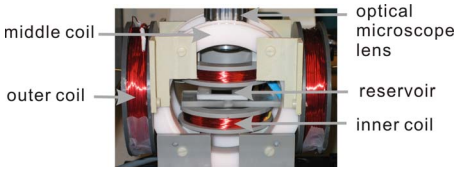

FIG. 2. (Color online) The experimental setup for the swimming tests of ABF using three-axis electromagnetic coils.

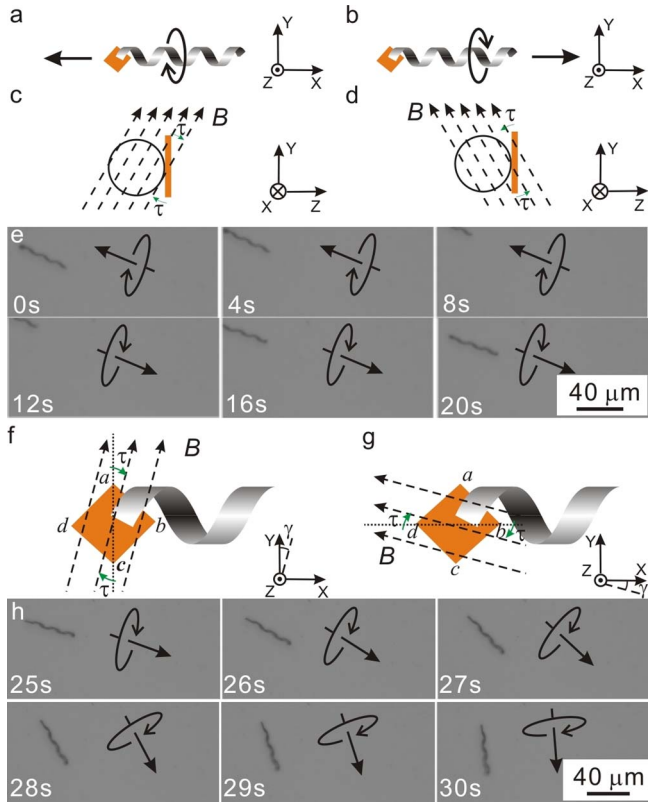

FIG. 3. (Color online) ABF swimming motion controlled by magnetic fields with field strength of 2.0 mT. [(a)–(d)] Schematic of a left-handed ABF swimming forward and backward. With the field B continuously rotating perpendicular to the X axis of the ABF, a misalignment angle between the field and the thin magnetic head will induce a magnetic torque (τ) that attempts to align the ABF head with the field, resulting in rotation and propulsion of the ABF. (e) Optical microscope images of the forward/backward motion of an ABF controlled by magnetic fields. The commanded translation and rotation directions of the ABF are indicated by the arrows. (f) If the field is rotated about the Z axis by an angle $|\gamma|<45°$ with respect to the easy axis $\overline{ac}$ of the head, then the ABF is steered as it is propelled, as the easy axis $\overline{ac}$ attempts to align with the field. This is the steering principle used during normal operation of the ABF. (g) If the field is rotated about the Z axis by an angle $|\gamma|<45°$ with respect to the easy axis $\overline{bd}$, the ABF will instantaneously attempt to rotate perpendicular to the helix axis. However, steering using the $\overline{bd}$ easy axis is not possible simultaneously with forward/backward propulsion. (h) Optical microscope images of the turning motion of an ABF controlled by magnetic fields. The commanded translation and rotation directions of the ABF are indicated by the arrows.

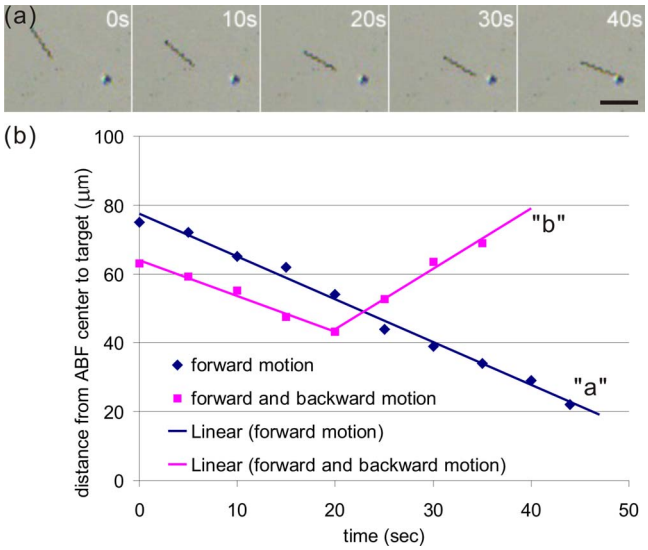

FIG. 4. (Color online) (a) A series of frames taken from a video showing an ABF driven toward a target in 40 s. The ABF has a 38 μm long InGaAs/GaAs helical tail with left-handed chirality. The scale bar is 40 μm for all images. (b) The experimental curves of the distance from the center point of the ABF to the target vs the time. Curve "a" shows the result from the ABF moving toward the target, i.e., (a). The forward velocity is 1.2 μm/s, corresponding to an angular speed of 6.3 rad/s. Curve "b" shows result from the same ABF moving forward at the initial 20 s and backward after that. The forward velocity is 1.1 μm/s and the backward velocity is 1.8 μm/s, corresponding to an angular speed of 6.3 rad/s and 10.5 rad/s, respectively.

count for swimming. To avoid the ABF sinking toward the substrate due to gravity, it is necessary to keep the ABF swimming with a positive pitch angle. In the experiments, a small pitch angle (10°–20°) is applied, with the required pitch angle being inversely proportional to velocity. Figure 4(a) show an ABF, with InGaAs/GaAs helical tail, swimming toward and reaching a target. The slope of a line fit to the data (curve "a") in Fig. 4(b) indicates the average velocity of the ABF is approximately 1.2 μm/s. Moreover, the forward motion of the ABF can be switched to backward motion by inverting the rotation direction of the magnetic field, e.g., from clockwise to counterclockwise, as shown in curve "b" of Fig. 4(b). The results indicate that the velocity increases linearly with the angular speed of the ABF.

Figure 5 demonstrates two basic manipulation tasks using an ABF, i.e., translation and rotation of microspheres. In Fig. 5(a), the image sequence shows an ABF pushing on one of two connected 6-μm-diameter polystyrene microspheres (Polysciences Inc.). The ABF is not rigidly connected to the

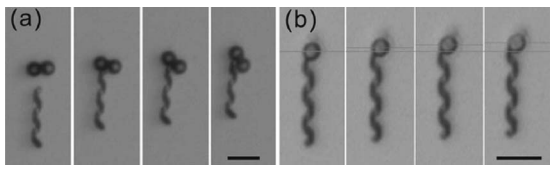

FIG. 5. (a) Two polystyrene microspheres are rotated 70° by a 29 μm long InGaAs/GaAs/Cr ABF pushing on one of the microspheres. The optical-microscope image sequence represents 2 s of elapsed time. (b) The microsphere is pushed for a radius length by the ABF within 1 s. The scale bars are 15 μm.

microsphere, but rather, swims toward it under human guided control. The image sequence shows that the ABF is able to rotate 70° the connected microspheres in 2 s. To estimate the thrust force of the ABF, a single microsphere was pushed [Fig. 5(b)]. Results show that the microsphere has a translational velocity of 3 μm/s when the angular speed of the ABF is 31.4 rad/s. In this low-Reynolds-number regime, the thrust force of the ABF is counterbalanced by the drag force of the microsphere in water, and the drag force of a sphere is expressed as[14]

$$F_{\text{thrust}} = F_{\text{drag}} = 3\pi\eta dv, \tag{1}$$

in which η is the viscosity of the water, and d and v are the diameter and velocity of the microsphere, respectively. Thus the thrust force of the ABF is calculated as 0.17 pN with an angular speed of 31.4 rad/s, and increases linearly with the angular speed.

In conclusion, ABF are untethered swimming microrobots that mimic bacterial flagella in both dimension and motion. The swimmer consists of an InGaAs/GaAs or InGaAs/GaAs/Cr helical tail and a thin soft-magnetic head. Experimental investigation has shown that ABF can be propelled and steered precisely in water by a low-strength, rotating magnetic field. These magnetically driven helical devices can be used as wireless manipulators for medical and biological applications under three-dimensional control in fluid environments, and have the potential to perform manipulation with a full 6 degrees of freedom.

The authors thank FIRST laboratory of ETH Zurich for technical support. We also wish to thank Magnus Hammer, Stefan Leutenegger, and Haixin Zhang for technical help. Funding for this research was partially provided by the Swiss National Science Foundation.

[1]G. T. Gillies, R. C. Ritter, W. C. Broaddus, M. S. Grady, M. A. Howard, and R. G. Mcneil, Rev. Sci. Instrum. **65**, 533 (1994).
[2]T. Honda, K. I. Arai, and K. Ishiyama, IEEE Trans. Magn. **32**, 5085 (1996).
[3]M. B. Khamesee, N. Kato, Y. Nomura, and T. Nakamura, IEEE/ASME Trans. Mechatron. **7**, 1 (2002).
[4]A. Yamazaki, M. Sendoh, K. Ishiyama, K. I. Arai, R. Kato, M. Nakano, and H. Fukunaga, J. Magn. Magn. Mater. **272–276**, E1741 (2004).
[5]K. B. Yesin, K. Vollmers, and B. J. Nelson, Int. J. Robot. Res. **25**, 527 (2006).
[6]E. M. Purcell, Am. J. Phys. **45**, 3 (1977).
[7]V. Y. Prinz, V. A. Seleznev, A. K. Gutakovsky, A. V. Chehovskiy, V. V. Preobrazhenskii, M. A. Putyato, and T. A. Gavrilova, Physica E (Amsterdam) **6**, 828 (2000).
[8]O. G. Schmidt and K. Eberl, Nature (London) **410**, 168 (2001).
[9]L. Zhang, E. Deckhardt, A. Weber, C. Schonenberger, and D. Grutzmacher, Nanotechnology **16**, 655 (2005).
[10]L. Zhang, E. Ruh, D. Grutzmacher, L. X. Dong, D. J. Bell, B. J. Nelson, and C. Schonenberger, Nano Lett. **6**, 1311 (2006).
[11]O. G. Schmidt, N. Schmarje, C. Deneke, C. Muller, and N. Y. Jin-Phillipp, Adv. Mater. (Weinheim, Ger.) **13**, 756 (2001).
[12]R. Dreyfus, J. Baudry, M. L. Roper, M. Fermigier, H. A. Stone, and J. Bibette, Nature (London) **437**, 862 (2005).
[13]F. B. Hagedorn and E. M. Gyorgy, J. Appl. Phys. **39**, 995 (1968).
[14]J. Happel and H. Brenner, *Low Reynolds Number Hydrodynamics* (Kluwer, Boston, 1983).